Comm. Korean Math. Soc. **15** (2000), No. 1, pp. 155–172

# ANALYTICAL AND NUMERICAL STUDY OF MODE INTERACTIONS IN SHOCK-INDUCED INTERFACIAL INSTABILITY

SUNG-IK SOHN

ABSTRACT. Mode interactions at unstable fluid interfaces induced by a shock wave (Richtmyer-Meshkov Instability) are studied both analytically and numerically. The analytical approach is based on a potential flow model with source singularities in incompressible fluids of infinite density ratio. The potential flow model shows that a single bubble has a decaying growth rates at late time and an asymptotic constant radius. Bubble interactions, bubbles of different radii propagates with different velocities and the leading bubbles grow in size at the expense of their neighboring bubbles, are predicted by the potential flow model. This phenomenon is validated by full numerical simulations of the Richtmyer-Meshkov instability in compressible fluids for initial multi-frequency perturbations on the unstable interface.

## 1. Introduction

When an incident shock collides with an interface between two fluids of different densities, it bifurcates into a transmitted shock and a reflected wave, while the interface becomes unstable. This interfacial instability is known as Richtmyer-Meshkov (RM) instability and plays a critical role in the design of inertial confinement fusion capsule. The dominant characteristics of an RM unstable interface are fingers, known as *bubbles* and *spikes*, of each phase extending into the region occupied by the opposite phase.

Received March 11, 1999. Revised September 1, 1999.

1991 Mathematics Subject Classification: 76B15, 76E30, 76L05.

Key words and phrases: interfacial instability, shock wave, potential flow, bubble, front tracking method.

The author wishes to acknowledge the financial support of the Korea Research Foundation made in the program year of 1997.

Thus, A bubble (spike) is a portion of the light (heavy) fluid penetrating into the heavy (light) fluid.

Since Richtmyer [1] proposed the linear theories for the RM instability, extensive research has been directed to solve this instability problem [2-8]. However, most studies were limited to simple initial conditions like pure sinusoidal perturbation of the interface. Only a few researchers have considered initial multi-frequency perturbations. The main purpose of this paper is to provide an analytical model for mode interactions at late nonlinear stages of the RM instability and validate the analytical model by full nonlinear numerical simulations for initial multi-frequency perturbations on the unstable interface.

The evolution of RM unstable interface with initial multi-frequency perturbations excite nonlinear interactions among different frequencies and much more complicated than that of initial single frequency perturbations. At the late nonlinear stage of multi-frequency perturbations, bubbles of different radii propagates with different velocities and the leading bubbles grow in size at the expense of their neighboring bubbles. This phenomenon is known as bubble interactions. The analytical model presented in this paper is a potential flow model with source singularity for the bubble interactions of the RM instability in incompressible fluids of an infinite density ratio.

We perform full numerical simulations of the RM instability in compressible fluids for initial multi-frequency perturbations on the unstable interface to investigate dynamics of the mode interactions and validate the potential flow model. The numerical simulation of the RM instability has been a challenging problem to researchers, since the problem involves complicated wave interactions of discontinuous waves and highly distorted interfaces. Most of previous published simulations of the RM instability were for the evolution of the initial single mode of an unstable interface [2, 6].

The numerical method used for simulations of mode interactions of the RM instability is the front tracking method [9]. The front tracking method is a well-established algorithm for tracking discontinuous fronts and interfaces and provides high resolutions of a front, avoiding oscillations behind a discontinuity.

In Section 2, we present a potential flow model for bubble interactions in incompressible fluids. Section 3 describes the front tracking method briefly and discuss the difficult aspects in the simulations of mode interactions of

the RM instability. Section 4 gives the results of the numerical simulations. Section 5 gives conclusions.

## 2. Analytical Model

In this section, we present an analytical model for bubble interactions of the RM instability, based on a potential flow with source singularities in incompressible fluids of an infinite density ratio. Even though, in reality, the RM instability occurs in compressible fluids, the incompressibility assumption is valid for the nonlinear stage. The author showed that the dynamics of RM unstable system changes from a compressible, approximately linear one to a nonlinear, approximately incompressible one [7].

We note that Richtmyer-Meshkov instability is closely related to the Rayleigh-Taylor (RT) instability (gravity induced instability) [10, 11, 12]. The similarity of these two instabilities is that they are interfacial instabilities induced by an external force (shock wave in RM case, and gravitational force in RT case). Kull proposed the potential flow model with a source singularity for the RT single bubble evolution [13] and Zufiria extended the Kull's potential flow model to the RT multiple bubble interactions [14]. We apply the Kull-type potential flow model to the RM bubble interactions.

### 2.1. Single Bubble Equations

First, we derive the equations for a single bubble evolution. Consider the bubble rising in a vertical channel filled with an incompressible irrotational inviscid flow. The density of the light fluid is zero. From the assumption of the flow, there exists a complex potential for the bubble $W(z) = \phi + i\psi$, where $\phi$ and $\psi$ are the velocity potential and the stream function, respectively. The bubble is characterized by the velocity of the bubble tip $U$, the local radius of curvature at the bubble tip $R$, and the location of the bubble tip $X$ with respect to a frame of reference attached to the channel.

The potential for the bubble can be modeled by the complex potential with a source singularity inside the bubble. Another potential flow model was proposed by Layzer [11]. Layzer applied the analytic velocity potential of a sinusoidal form for the bubble evolution and obtained a result for the limiting velocity of the RT bubble. Layzer's model has been extended

to the RM bubble by Hecht *et al.* [5]. However, as Layzer pointed out in his paper, the bubble should be modeled by the potential with source singularity. Furthermore, Kull showed that the potential with source singularity (Eq. (4)) is a generalization of the Layzer's model of a sinusoidal velocity potential and contains the result of the sinusoidal velocity potential in some limits of the parameters in steady state case [13].

The potential with a source singularity gives a nice description for the front of the bubble, but is not correct for the flow in the far field behind the bubble. The source potential gives a constant velocity at the far field behind the bubble. However, in reality, the spikes are formed in the flow. Therefore, our model assumes that the spike gives a little influence to the dynamic of the bubble. This assumption of a negligible effect of the spike is supported by the agreement of our model with the results of numerical simulations for full Euler equations in Section 4.

We describe the evolution in a comoving frame $(\hat{x}, \hat{y})$ rising with the bubble. Then the origin of coordinate $(\hat{x}, \hat{y})$ is attached to the bubble tip $x = X(t), y = L/2$ moving with the bubble velocity $U$ in the $x$ direction, where $L$ is a channel width (see Fig. 1). The bubble shape in the neighborhood of the bubble tip is approximated to second order [15]:

$$\eta(\hat{x}, \hat{y}, t) = \hat{y}^2 + 2R(t)\hat{x} = 0. \tag{1}$$

The bubble evolution can be determined by the kinematic boundary condition

$$\frac{D\eta(\hat{x}, \hat{y}, t)}{Dt} = 2\frac{dR}{dt}\hat{x} + 2Ru + 2\hat{y}v = 0 \tag{2}$$

and the Bernoulli equation

$$\frac{\partial \phi}{\partial t} + \frac{1}{2}(\nabla\phi)^2 + g\hat{x} + \frac{dU}{dt}\hat{x} = 0 \tag{3}$$

where $u$ and $v$ are the $\hat{x}$ and $\hat{y}$ component of fluid velocity in the comoving frame with the vertex of the bubble, respectively, and $g$ is an external acceleration.

The potential for a source is described by $W = Q \log \hat{z}$ where $Q$ denotes the source strength. Then, the potential of a source at the origin in a channel of width $L$, $W = Q \log [\sinh(\pi\hat{z}/L)]$, can be derived by Schwarz-Christoffel transformation [16]. Combining a source located at a distance

$A$ below the bubble tip with a uniform incoming flow, we obtain the resulting source potential for the bubble

$$W(\hat{z}) = Q \log\left[\frac{\sinh\frac{k}{2}(\hat{z}+A)}{\exp\frac{k}{2}(\hat{z}+A)}\right] - U\hat{z}. \tag{4}$$

Here $k$ is a characteristic wave number defined as $k = 2\pi/\lambda$ where $\lambda = L$ denotes a channel width. The velocity potential and the stream function are given by

$$\phi = \frac{Q}{2}\log[\cosh k(\hat{x}+A) - \cos k\hat{y}] - (\frac{1}{2}kQ + U)\hat{x}, \tag{5}$$

$$\psi = Q\arctan[\coth\frac{k}{2}(\hat{x}+A)\tan\frac{k}{2}\hat{y}] - (\frac{1}{2}kQ + U)\hat{y}. \tag{6}$$

Notice that $\phi \to -U\hat{x}$ as $\hat{x} \to +\infty$, and $\phi \to -e^{kA}U\hat{x}$ as $\hat{x} \to -\infty$, from Eq. (5) and $\log[\cosh k(\hat{x}+A)] \sim -k\hat{x}$ as $\hat{x} \to -\infty$.

Expanding (4) in powers of $\hat{z}$, we have

$$W = Q\sum_{i=0}^{\infty}\frac{c_i}{i\,!}\hat{z}^i - U\hat{z}. \tag{7}$$

The expressions for coefficients $c_i$ are given shortly.

From the relation $\frac{dW}{d\hat{z}} = u - iv$ and Eq. (1) and (7), the velocity $u$ and $v$ are

$$u = Q[c_1 + (c_2 + c_3R)\hat{x}] - U + O(\hat{x}^2), \tag{8}$$

$$v = -c_2Q\hat{y} + O(\hat{x}^{3/2}). \tag{9}$$

Substituting (8) and (9) into Eq. (2), and the zeroth and first order equations in $\hat{x}$ gives

$$\frac{dX}{dt} = U = c_1Q, \tag{10}$$

$$\frac{dR}{dt} = -Q(3c_2 + c_3R)R. \tag{11}$$

Substituting expansions in powers of $\hat{x}$ for (5), or real part of (7), the first and second order equations in $\hat{x}$ gives

$$(c_1 + c_2R)\frac{dQ}{dt} + Q(c_2 + c_3R)\frac{dA}{dt} = Q^2c_2^2R - g, \tag{12}$$

$$(13)\qquad (\frac{c_2}{2}+c_3R+c_4\frac{R^2}{6})\frac{dQ}{dt}+Q(\frac{c_3}{2}+c_4R+c_5\frac{R^2}{6})\frac{dA}{dt}$$
$$=-\frac{Q^2}{2}\left(c_2^2-2c_2c_3R+(3c_3^2-4c_2c_4)\frac{R^2}{3}\right),$$

using the fact $\frac{d}{dt}c_i = c_{i+1}\frac{dA}{dt}$, $i \geq 1$. Here, the expressions for $c_i$ are

$$c_1 = \frac{k}{e^{kA}-1}, \qquad c_2 = -\frac{k^2e^{kA}}{(e^{kA}-1)^2},$$
$$c_3 = \frac{k^3e^{kA}(e^{kA}+1)}{(e^{kA}-1)^3}, \qquad c_4 = -\frac{k^4e^{kA}(e^{2kA}+4e^{kA}+1)}{(e^{kA}-1)^4},$$
$$c_5 = \frac{k^5e^{kA}(e^{3kA}+11e^{2kA}+11e^{kA}+1)}{(e^{kA}-1)^5}.$$

The evolution of a single bubble is determined by the system of four first order ordinary differential equations (10), (11), (12) and (13) with given initial conditions.

The streamline through an arbitrary reference point $(\hat{x_0}, \hat{y_0})$ is defined by $\psi(\hat{x}, \hat{y}, t) = \psi(\hat{x_0}, \hat{y_0}, t)$. Figure 1 is a streamline pattern for a single bubble system. The source is located at the $\hat{x} = -A, \hat{y} = 0$, and the curve obtained by the streamline $\psi = 0$ through the stagnation point at $\hat{x} = \hat{y} = 0$ determines the bubble profile. The analytic expression of the bubble profile is found to be

$$(14)\qquad y = \frac{1}{k}\log\left[\frac{\sin(\epsilon kx)}{\sin(\alpha\epsilon kx)}\right] - A.$$

where $\alpha = e^{-kA}$ and $\epsilon = \frac{1}{1-\alpha}$.

Now, we show the results for the RM single bubble evolution. We consider the Eqs. (10), (11), (12) and (13) with $g = 0$. This is an impulsive approximation for an incompressible flow. We use a fourth-order Runge-Kutta method to solve the Eqs. (10), (11), (12) and (13).

The results of the RM single bubble evolution are given in Figure 2 for the initial conditions $R = 0.2, Q = 0.1, A = 0.1$. The channel width is $L = \pi$. The bubble profiles are determined by Eq. (14). The curves from the bottom to the top correspond to the bubble profiles for $t = 0, 2, 4, 6, 8, 10$. Fig. 2 shows that the growth rates are large at early times and become smaller at late times.

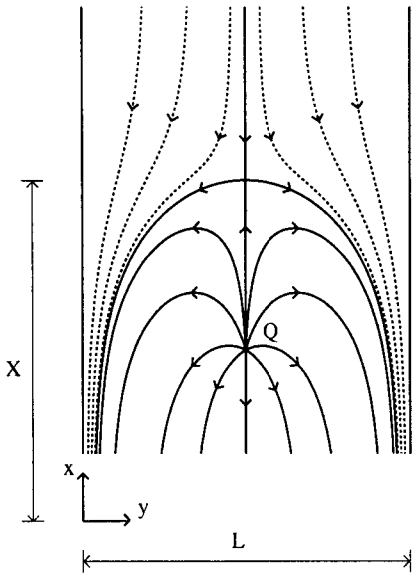


FIGURE 1. Streamline pattern of a potential flow model with source singularity. The curve emanated from the stagnation point at $\hat{x} = \hat{y} = 0$ determines the bubble profile, and the source is located at the $\hat{x} = -A, \hat{y} = 0$.

Figure 3 gives the results of state variables in the RM single bubble evolution for the same initial conditions as the ones in Fig. 2. Figure 3 shows that the bubble velocity $U$ and the source strength $Q$ decay to zero, and the local radius of the bubble $R$ and the distance of the source from the bubble tip $A$ reach the values 1.30 and 1.33, respectively. We have checked that, for any positive initial conditions, $R$ and $A$ have a steady state solution $R^{\infty} = 1.30$ and $A^{\infty} = 1.33$, and $U$ and $Q$ decay to zero asymptotically. Recently, Hecht *et al.* determined an asymptotic bubble growth rate of $2/(3kt)$, based on the Layzer's model of an analytic velocity potential [5]. In Fig. 3(a), we compare this asymptote with our result of the bubble velocity. It shows two solutions are in a good agreement at late times.

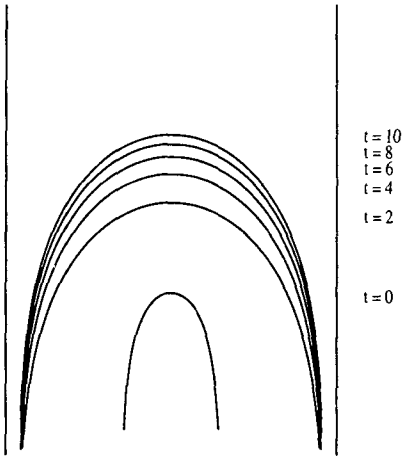


FIGURE 2. Single bubble evolution of Richtmyer-Meshkov instability for the initial conditions $R = 0.2, Q = 0.1, A = 0.1$.

The analogous results for the RT case ($g$=constant) are previously studied in [13, 14] and it has been found that the single-mode RT bubble attains a constant asymptotic velocity and a constant asymptotic radius. It is interesting to note that the RM asymptotic bubble radius, $R^{\infty}_{\mathrm{RM}} = 1.30$, is larger than the RT asymptotic bubble radius, $R^{\infty}_{\mathrm{RT}} = 0.866$ [14].

## 2.2. Multiple Bubble Equations

Next, we consider bubble interactions. Assume that $N$ distinct bubbles rise in a channel of width $L$ with the walls as axes of symmetry and the positions of the bubble tips are $Z_m = X_m + iY_m, m = 1, 2, \cdots, N$.

We neglect the lateral effects and assume $Y_m$ are constants. Since each bubble is described by a potential with source singularity, the potential for multiple bubbles can be constructed as the sum of the potentials of all bubbles with source singularity located at $Z_m - A_m, m = 1, 2, .., N$ [14, 16]. Then, rearranging (4) and applying the method of image, the resulting potential in a comoving frame with the $m$-th bubble tip is

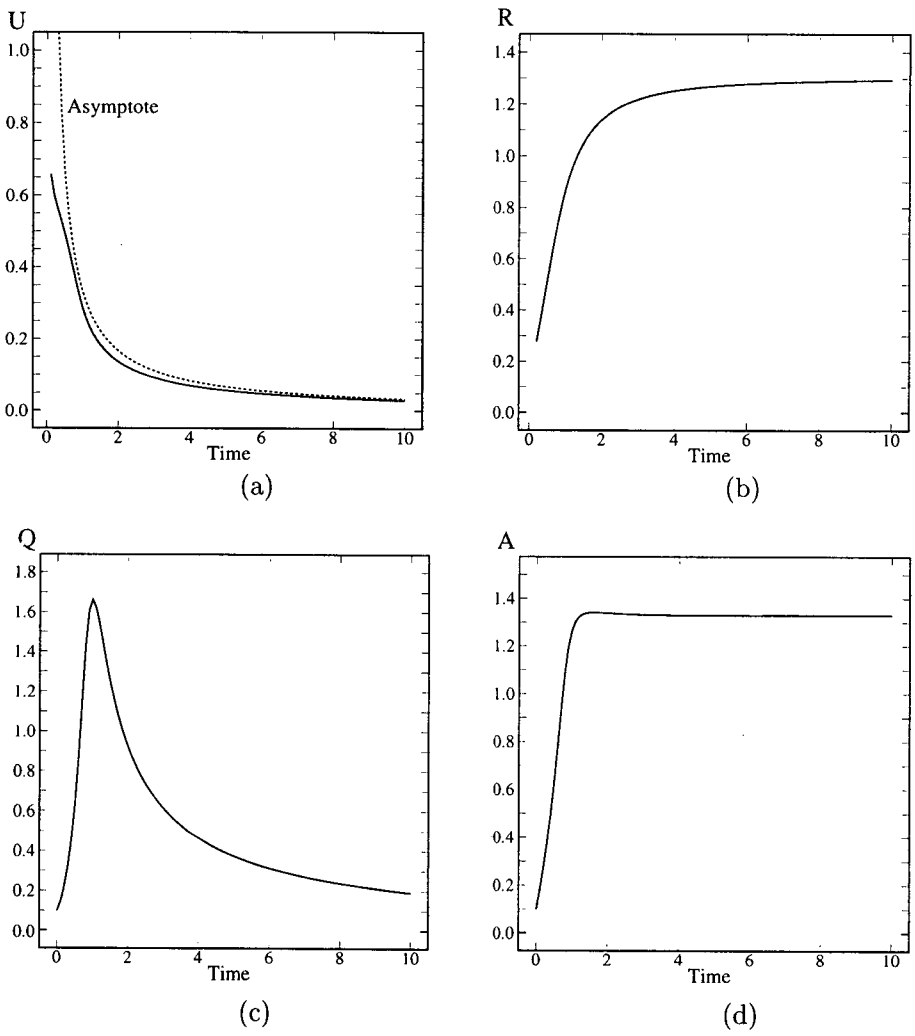


FIGURE 3. The results of the single bubble evolution in the RM instability for the initial conditions $R = 0.2, Q = 0.1, A = 0.1$. (a) bubble velocity $U$ and asymptote of bubble growth rate $2/(3kt)$, (b) Radius of the bubble tip $R$, (c) Source strength $Q$, (d) Distance of the source from the bubble tip $A$.

$$(15)\, W_m(\hat{z}) = \sum_{j=1}^{N} Q_j \log[(1 - e^{\frac{k}{2}(Z_j - A_j - Z_m - \hat{z})})(1 + e^{\frac{k}{2}(Z_j^* - A_j - Z_m^* - \hat{z})})] - U_m \hat{z}$$

where the star denotes the complex conjugate.

Satisfying Eq. (2) and (3) with the potential (15), we can develop a set of $4N$ system of ordinary differential equations for $U_m, R_m, Q_m$ and $A_m$ which describe the motion of the $N$ bubbles. The initial conditions for the longitudinal locations of bubbles $X_m$ are perturbed from zero to generate the interaction and the ones for the horizontal locations of bubbles $Y_m$ are equally spaced values of the channel width. The initial conditions for $R_m, A_m$ are scaled steady state solutions of the single bubble: $R_m = \frac{R^\infty}{N}, A_m = \frac{A^\infty}{N}$ for $m = 1, .., N$; the initial conditions for $Q_m$ are arbitrary given.

The equations are applied to the case of two bubble interactions ($N = 2$) as a simple model of multiple bubble interactions. Figure 4 shows the results of bubble tip positions and local radius of bubbles in RM two bubble interactions in the channel of width $L = \pi$. Initially, $X_2$ is moved back from zero by 5% of the radius of middle bubble $R_2$. The perturbation in the size of the bubble has same effect as a perturbation in the longitudinal location of the bubble.

Fig. 4 clearly demonstrates the bubble interaction process. In Fig. 4 (a), we see that the two bubbles advance and compete for a while. The higher bubble grows faster than the other, since it has more free space, and finally attains the asymptotic velocity of a single bubble. The lower bubble grows slower, and reaches a possible maximum, and then is washed downstream. Fig. 4 (b) shows that the higher bubble expands, while the lower bubble shrinks and recovers its size at later times. The higher bubble finally attains the asymptotic radius of a single bubble, $R^\infty_{\mathrm{RM}} = 1.3$. Therefore, the front of channel is eventually filled with the higher bubble. On the other hand, the smaller (or, lower) bubble tends to recover its size when it is in the far downstream. This result is due to the incorrect description of our model for the flow in the far field behind the bubble. It is mentioned that, in reality, the spikes are formed at the back of the bubble and the smaller bubble merge into the spike region. We can see that the dynamics in the far field give a little influence to the motion of the front bubble. This result is validated in the full numerical simulations in Section 4. The

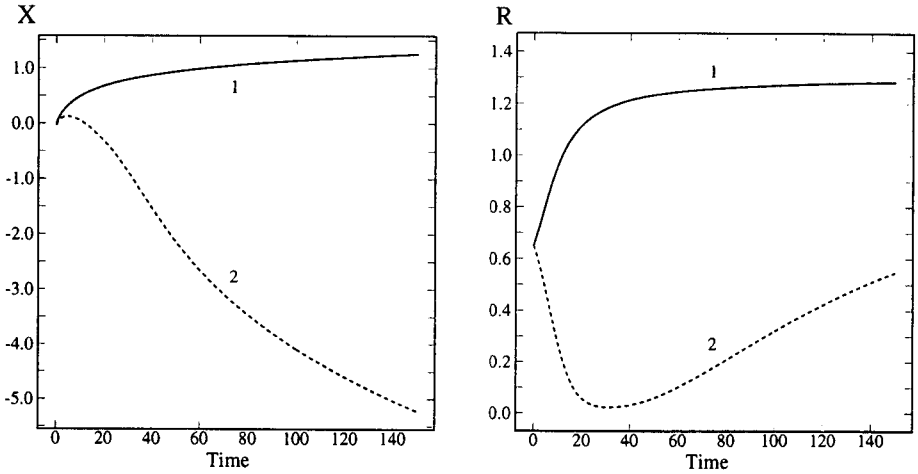


FIGURE 4. The results of two bubble interactions in the RM instability. (a) Height of bubbles, (b) Radius of bubbles.

behavior of recovering the size of the smaller bubble also occurs in the potential flow model for the RT instability [14]. Therefore, the overall bubble interaction process of the RM instability is qualitatively similar to the one of the RT instability, although the growth rate of the front bubble is different.

## 3. Numerical Method

We apply the front tracking method for full numerical simulations of mode interactions of the RM instability in compressible fluids to validate the theoretical results obtained in Section 2.

The fluid motion of the Richtmyer-Meshkov instability in compressible fluids can be described by the inviscid Euler equations [17], that is

$$\frac{\partial \rho_j}{\partial t} + \frac{\partial(\rho_j u_j)}{\partial x} + \frac{\partial(\rho_j v_j)}{\partial y} = 0, \tag{16}$$

$$\frac{\partial(\rho_j u_j)}{\partial t} + \frac{\partial}{\partial x}(\rho_j u_j^2 + p) + \frac{\partial}{\partial y}(\rho_j u_j v_j) = 0, \tag{17}$$

$$\frac{\partial(\rho_j v_j)}{\partial t} + \frac{\partial}{\partial x}(\rho_j u_j v_j) + \frac{\partial}{\partial y}(\rho_j v_j^2 + p) = 0, \tag{18}$$

$$\frac{\partial(\rho_j E_j)}{\partial t} + \frac{\partial}{\partial x}[u_j(\rho_j E_j + p)] + \frac{\partial}{\partial y}[v_j(\rho_j E_j + p)] = 0. \tag{19}$$

Here $\rho$ is the density, $u$ the $x$-components of the velocity, $v$ the $y$-components of the velocity, $p$ the pressure; $E$ the specific total energy. The index $j = 1, 2$ distinguished components of fluids on each side of the interface. Eq. (16) is conservation of mass, Eqs. (17)-(18) are conservation of momentum in the $x, y$ directions, respectively, and Eq. (19) is conservation of energy. The system is closed by specifying equations of state. We use the equations of state for a polytropic gas,

$$E_j = \frac{1}{(\gamma_j - 1)}\frac{p}{\rho_j} + \frac{u_j^2 + v_j^2}{2}, \tag{20}$$

where $\gamma$ is the polytropic exponent.

We solve the hyperbolic system of Eqs. (16)-(20) by the front tracking method. The front tracking method has been developed over the years by a group of researchers [9, 18, 20] and has been successfully applied to a wide variety of problems having sharp interface or wave fronts which include gas dynamics, porous media, solid mechanics [9, 19, 20, 21]. Here we briefly describe the algorithm of the front tracking method for compressible gas dynamics.

In the front tracking method, the propagation of the solution to the next time step is divided into two main parts: the propagation of the tracked wave structures (front propagation) and the updating of the state values at locations away from the tracked front (interior propagation). Since the solution of the front tracking is divided into two parts, two different type of grid should be constructed. These two grids consist of a standard rectangular finite difference grid for interior solutions and a mobile lower dimensional grid for the tracked fronts.

The state values of all interior points are computed by using common shock capturing schemes such as the Lax-Wendroff method with artificial viscosity or the MUSCL scheme [22].

The front propagation is the algorithm to propagate marked points on the tracked fronts. For each front the operator is split into the normal and tangential sweeps over its points. At first, the point propagation algorithm is constructed using solutions to Riemann problems. A Riemann

problem for an one-space-dimensional system is an initial value problem with piecewise constant initial data and a single jump discontinuity. We first solve the equation given by the component of Eqs. (16)-(19) in the normal direction of the tracked front with two states on either side of the traced wave for initial data of a Riemann problem. The solution to this Riemann problem provides both the (predicted) wave speed in the normal direction of the traced wave, and a pair of (predicted) time-updated states on the curve. The state values obtained by the Riemann problem solutions are corrected by the method of the characteristics and the Rankine-Hugoniot conditions. The tangential components of the state at the front can be obtained by solving an initial value problem of the corresponding tangential components of Eq. (16)-(19).

An intersection of two or more curves of an interface is defined as a node. The evolution of nodes are determined by the solution of a two-dimensional Riemann problem. Various node types have been classified and their propagation algorithms have been implemented by using shock polar analysis [18].

The front tracking simulation for the evolution of the initial single mode of the RM instability was studied by Holmes *et al.* [6]. However, The simulation for initial multi-frequency modes of the RM unstable interface by the front tracking method is more difficult than the one for single mode case, since it involves the interactions of tracked waves. These interactions include the tangling of tracked waves, the collision of nodes, and the bifurcation of a single node.

Tangling occurs when two or more wave intersect after propagation. Wave tangles are classified according to the type of the intersecting waves. Standard types of wave tangles are boundary tangle, contact discontinuity tangle, and shock-contact discontinuity tangle. Node interactions are detected if the node propagation algorithm fails due to the blocking of a node by nearby nodes. Node interactions include the crossing of a wave around a corner, the crossing of a node through a periodic boundary, and collision of two nodes. A node bifurcation is a node interaction where a single node breaks up into a more complex configuration. Each type of wave interactions requires a specialized propagation algorithm. We refer to [20] for the details of wave interactions and the algorithms.

We have checked that turning off tracking and using shock capturing, to avoid the computations of complicated wave interactions, lead to a dramatic reduction in resolution of the computation around the interacting

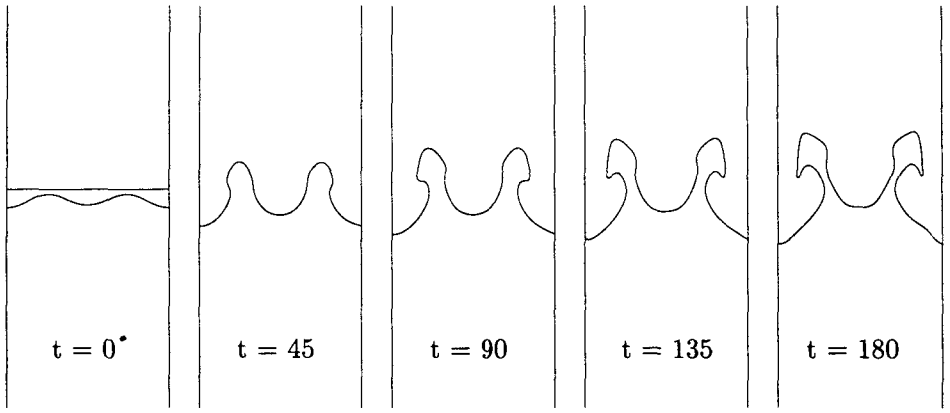


FIGURE 5. The interface evolution for a two bubble simulation. At $t = 0$, the radii of the bubble in the middle to the bubble in the wall are same and the heights are in the ratio 0.88:1. The vertical wall is a periodic boundary. The shock of Mach number 1.2 incidents from light to heavy fluid. The nondimensional time is defined as $k\tau_0 M_0 t$. Here $\tau_0$ is the speed of sound ahead of the incident shock, and $M_0$ is the Mach number of the incident shock.

waves. Therefore, the tracking for the wave interactions must be taken for the high resolution of the computation.

## 4. Numerical Results

After the incident shock collides with the contact interface, the transmitted shock and the reflected shock move fast in opposite directions. Since the effect of the the transmitted shock and the reflected shock should be considered and the mode interactions of the RM instability occurs at late times, the numerical simulation requires a long computational domain. This fact drastically increases the computation cost.

Figure 5 shows the result of the front tracking simulation for the two bubble interactions of the RM instability. The radii of the small bubble to the large bubble are same and the heights are in the ratio 0.88:1. The

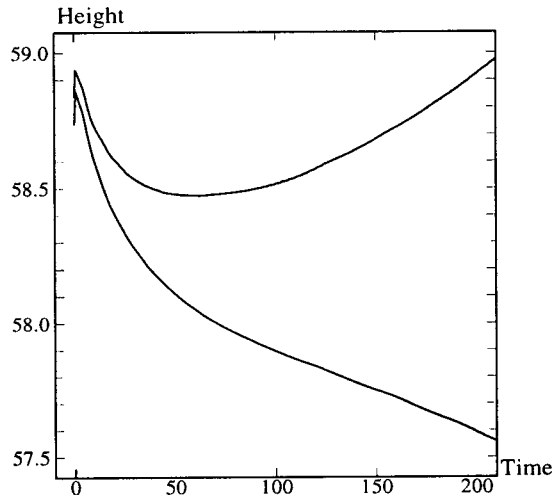


FIGURE 6. The plot of bubble heights versus time for the simulation of two bubble interactions.

vertical wall is a periodic boundary. The density ratio of two fluids is 1:5, and the adiabatic exponents are $\gamma_1 = 1.4$ for the upper fluid and $\gamma_2 = 1.094$ for the lower fluid. The compressible interface is accelerated by a weak shock of Mach number 1.2 moving downward. The reflected wave is a shock.

The computational domain is $2\pi \times 80\pi$ in a nondimensional unit. The time $t$ and length $x$ are nondimensionalized by $k\tau_0 M_0 t$ and $kx$, respectively. Here $\tau_0$ is the speed of sound ahead of the incident shock and $M_0$ is the Mach number of the incident shock. The interface actually moves downward after the collision with the incident shock. Here, to reduce the computation cost, we deduct the velocity fields by the velocity jump after the incident shock passage. Fig. 5 is a partial view around the contact interface, not a whole computational domain. Fig. 5 shows that the bubble interactions, the advanced bubble grows faster than behind bubble and expands, and the behind bubble is pushed back and shrinks, do occur in the RM instability in compressible fluids. Fig. 5 also shows that the interface have two spikes and the vortex structures due to discontinuity of tangential velocities at the spikes are formed around $t \approx 90$, the time when the smaller bubble begins to be pushed back.

In Figure 6, we plot the bubble tip locations for the Fig 5. Fig. 6 shows that the initially advanced bubble grows faster than the other, while the behind bubble initially moves forward, but grows slower than the front bubble, and is pushed back finally. This result agrees with the theoretical predictions of the potential flow model in Section 2. The agreement between the results of the potential flow model and the numerical simulation indicates that the evolution of bubbles may not be affected by the motion of spikes.

## 5. Conclusions

In this paper the potential flow model in which bubbles are described by point sources are applied to study the bubble interactions of the RM unstable interface in incompressible fluids of an infinite density ratio and are validated by the full numerical simulation of the the RM instability in compressible fluids for initial multi-frequency perturbations on the interface.

The potential flow model predicts the behavior of a single bubble of decaying growth rate and an asymptotic constant radius, and the bubble interaction process of the RM instability. It is found that, in the bubble interaction, a larger bubble finally attains the asymptotic velocity and asymptotic radius of a single bubble. The numerical simulation, using the front tracking method, is in a good agreement with the result of the potential flow model, and it shows that the potential flow model gives a good qualitative description for the bubble interaction of the RM instability.

The numerical simulation of the RM instability for the case of the randomly perturbed interface and a comparison with the multiple bubble interactions of the potential flow model will be interesting for practical fusion problems and will be the next step of the research.

ACKNOWLEDGEMENT. The author would like to thank the referee for his careful reading and helpful comments.

## References

[1] R. D. Richtmyer, *Taylor instability in shock acceleration of compressible fluids*, Comm. Pure Appl. Math. **13** (1960), 297-319.

[2] K. A. Meyer and P. J. Blewett, *Numerical investigation of the stability of a shock-accelerated interfaces between two fluids*, Phys. Fluids **15** (1972), 753-759.

[3] G. Fraley, *Rayleigh-Taylor stability for a normal shock wave-density discontinuity interaction*, Phys. Fluids **29** (1986), 376-386.

[4] Y. Yang, Q. Zhang, and D. H. Sharp, *Small amplitude theory of Richtmyer-Meshkov instability* , Phys. Fluids A **6**, (1994), 1856-1873.

[5] J. Hecht, U. Alon and D. Shvarts, *Potential flow models of Rayleigh-Taylor and Richtmyer-Meshkov bubble fronts*, Phys. Fluids **6** (1994), 4019-4030.

[6] R. L. Holmes, J. W. Grove and D. H. Sharp, *A numerical investigation of Richtmyer-Meshkov instability using front tracking*, J. Fluid Mech. **301** (1995), 51-64.

[7] Q. Zhang and S.-I. Sohn, *Nonlinear solutions of unstable fluid mixing driven by shock waves*, Phys. Fluids **9** (1997), 1106-1124.

[8] ———, *Quantitative theory of Richtmyer-Meshkov instability in three dimensions*, Zeit. angew. Math. Phys. **50** (1999), 1-46.

[9] I.-L. Chern, J. Glimm, O. McBryan, B. Plohr and S. Yaniv, *Front tracking for gas dynamics*, SIAM J. Sci. Stat. Comput. **7** (1986), 83-110.

[10] G. I. Taylor, *The instability of liquid surfaces when accelerated in a direction perpendicular to their planes I*, Proc. R. Soc. London A **201** (1950), 192-196.

[11] D. Layzer, *On the instability of superimposed fluids in a gravitational field*, Astrophys. J. **122** (1955), 1-12.

[12] P. R. Garabedian, *On steady-state bubbles generated by Taylor instability*, Proc. R. Soc. London A **241** (1957), 423-431.

[13] H. J. Kull, *Nonlinear free-surface Rayleigh-Taylor instability*, Phys. Rev. A **33** (1986), 1957-1967.

[14] J. Zufiria, *Bubble competition in Rayleigh-Taylor instability*, Phys. Fluids **31** (1988), 440-446.

[15] J.-M. Vanden-Broeck, *Bubbles rising in a tube and jets falling from a nozzle*, Phys. Fluids **27** (1984), 1090-1093.

[16] L. M. Milne-Thompson, *Theoretical hydrodynamics*, Dover, New York, (1968).

[17] R. Courant and K. O. Friedrich, *Supersonic flow and shock waves*, Springer-Verlag, New York, (1976).

[18] J. Glimm, C. Klingenberg, O. McBryan, B. Plohr, D. Sharp and S. Yaniv, *Front tracking and two dimensional Riemann problems*, Adv. Appl. Math. **6** (1985), 259-290.

[19] J. Glimm, X. L. Li, R. Menikoff, D. H. Sharp and Q. Zhang, *A numerical study of bubble interactions in Rayleigh-Taylor instability for compressible fluids*, Phys. Fluids A **2** (1990), 2046-2054.

[20] J. Grove, *Applications of front tracking to the simulation of shock refractions and unstable mixing*, Appl. Num. Math. **14** (1994), 213-237.

[21] H.-C. Hwang, *On the numerical methods for discontinuities and interfaces*, Comm. Kor. Math. Soc. **13**, (1998), 655-682.

[22] B. van Leer, *Towards the ultimate conservation difference scheme. V. A second-order sequel to Godunov's method*, J. Comp. Phys. **32** (1979), 101-136.

School of Information Engineering
Tongmyong University of Information Technology
Pusan 608-711, Korea
*E-mail*: sohnsi@tmic.tit.ac.kr